TECHNICAL PAPER

Design of a 2-DOF scanning mirror using flexible membrane and electromagnetic actuators

Shuaiby Mohamed[1,2] · Ejaz Ahmad[2] · YoungWoo Im[2] · Wan-Chin Kim[3] · Youngshik Kim[2] · Buhyun Shin[2]

Abstract

Micromirrors play a vital role in various fields, including vision systems, optical networking, and laser projects. In this paper, we developed a 2-DOF scanning mirror using flexible membrane and electromagnetic actuator. We have developed two flexible membranes in the sine and pulse shapes, each with a simple and compact structure using 3D printing technology. As a driving mechanism, we developed an unique electromagnetic actuator consisting of two pairs of coils and cross shaped yoke and one permanent magnet. To analyze the magnetic flux in the electromagnetic system, we employed finite element analysis. We conducted experiments with the proposed system with dimensions of 24 mm (width) $\times$ 24 mm (depth) $\times$ 20 mm (height), which corresponds to a mirror with a radius of 3 mm. We conducted experiments and simulations with both flexible membranes in our study. The experimental results show that when an input voltage is $\pm$ 5 V, the system using a pulse-shaped membrane achieves a rotation angle $\pm$ 3° at the bandwidth of 15 Hz. The proposed 2-D scanning mirror offers significant advantages in terms of its compact, low production cost and simple design.

1 Introduction

2-D scanning mirrors are used in a variety of industries where exact control over a laser or light beam's direction is necessary. Usually, it consists of two mirrors that are positioned on orthogonal axes and can be tilted or rotated to change the direction of light that is reflected. Due to its vast applications, an extensive amount of research is carried out on 2-D scanning mirrors using micro-electrical mechanical systems (MEMS) (Khatokar et al. 2021; Qi et al. 2018; Chen et al. 2022; Zhou et al. 2021; Koh and Lee 2012; Mao et al. 2022). Their appropriateness for high-performance scientific instrumentation was examined and demonstrated in Anderson et al. (2021) and Mao et al. (2022), where a particular micro-mirror component's suitability was assessed using a specially designed optical bench setup to assess large-scale linear response, pointing precision, thermal drift and stability, and temporal stability. To address the absence of feedback control of the micro-mirrors and enable in vivo operation, a micro-mirror was devised by Tanguy et al. (2017) to improve the stability of the in-frame mirror and give broad scanning ranges over a large bandwidth at low driving voltage. In Samanta et al. (2022), the authors proposed electrothermally scanning mirror at high speeds, they were able to achieve ringing-free, linear, and consistent control. There are other types of scanning mirrors, including piezoelectrically driven (Cheng et al. 2023; Gilchrist et al. 2012; Hwang et al. 2024; Gilchrist et al. 2009; Koh et al. 2011; Senger et al. 2021) and electrostatically driven mirrors (Zara et al. 2003;

✉ Buhyun Shin
  jedidiah@hanbat.ac.kr

  Shuaiby Mohamed
  shuaiby.mohamed@aun.edu.eg

  Ejaz Ahmad
  ejaz.msee@gmail.com

  YoungWoo Im
  leyoungwoo@naver.com

  Wan-Chin Kim
  wckim97@hanbat.ac.kr

  Youngshik Kim
  youngshik@hanbat.ac.kr

1   Department of Mechatronics Engineering, Faculty of Engineering, Assiut University, 71516 Asyût, Egypt

2   Department of Mechanical Engineering, Hanbat National University, 34158 Daejeon, Korea

3   Department Mechanics-Materials Convergence System Engineering, Hanbat National University, 34158 Daejeon, Korea

Jin et al. 2011; Conant et al. 2000; Hung et al. 2015). The authors in Cheng et al. (2023) presented piezoelectrically driven scanning mirrors to be used in LiDAR vehicles. A closed-loop control is developed based on piezoelectrically driven mirrors to deal with the position-sensing signals (Senger et al. 2021). Using the Lissajous scan pattern, the work (Hung et al. 2015) proposed an electrostatically powered bi-axial micro scanner with capacitive position sensing for projection display to provide position signals for mirror to achieve image projections.

A large area MEMS tip-tilt micro-mirror was designed and fabricated by Sadhukhan and Singh (2022) to attain a bi-axial optical displacement and specific vibration frequency with a serpentine beam architecture. By using an avalanche photodiode as a photodetector, the study (Yangyang and Qian 2019) proposed a 2-D scanning range-finding LIDAR based on MEMS mirror and STM32 to direct a nanosecond pulsed beam in terms of time-of-flight measurement. A two-axis scanning mirror microsystem that is specially made for dependable and quick underwater scanning of both optical and ultrasonic beams has been shown by Huang et al. (2013). To satisfy the demands of high-performance raster scanning mirrors for retinal scanning displays and imaging applications, a microelectromechanical systems actuation technique is developed in Yalcinkaya et al. (2006) that effectively drives a two-axis scanning mirror to wide angles at high frequency. In order to create 2-D optical scanning trajectories, the research work proposed in Ito et al. (2023) modeling-free inversion-based iterative control for a fast steering mirror, a dual-input dual-output system.

An electromagnetic driven biaxial scanning mirror and its use in an HD laser projection system was proposed (Yu et al. 2021). This mirror can provide the necessary large-angle driving moment and high frequency. A 2-D imaging method proposed in Zhang et al. (2023) to avoid zero-interpolation and zero-padding, saving computing burden, by dealing directly with spatial-frequency domain data through the use of a $(\sin\theta - R)$ coordinate system. The authors in Csencsics and Schitter (2017) presented a way to align the driving frequencies of the intended Lissajous scanning trajectory with the resonance frequencies of the system axes, thereby increasing the possible scan range and improving the energy efficiency. To increase a scanning mirror's angular deflection accuracy, a model-based angle-correction technique was devised and validated in Fan et al. (2019). In our previous work (Hyun et al. 2013), we presented a miniature scanning mirror system for the decoupled 2-D motions that uses electromagnetic actuators and a simple driving framework. Similarly, in Shin et al. (2018) we designed a compact, low-power LIDAR with a high rotation angle and low resonance frequency biaxial scanning mirror. Electromagnetic drive has the benefit of
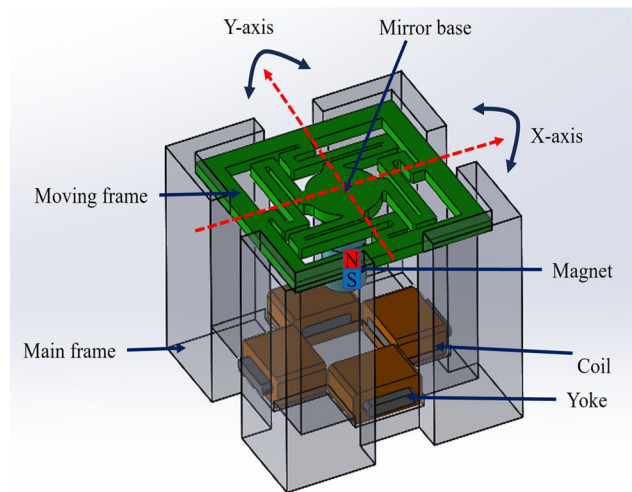

Fig. 1 3D model of the proposed system

not requiring electrical connections and being simply constructed using microfabrication processes (Mohamed et al. 2024). It operates by means of an external coil. Because of its wide commercial use and more linear response when compared with other concepts, this type of actuation is particularly well-suited for linear slow scanners.

The aim of this study is to develop a biaxial scanning mirror capable of achieving a low resonance frequency and a significant rotation angle. To fulfill these objectives, we designed and fabricated a custom electromagnetic actuator specifically designed for a biaxial scanning mirror, meeting the desired specifications. The electromagnetic actuator that was developed in this study exhibits impressive characteristics, including a wide deflection angle and rapid response. We developed two flexible membranes with a simple and compact structure using 3D printing technology.

The remaining sections of this paper are organized as follows: the design of a scanning micro-mirror is explained in Sect. 2. The dynamic model of the system is descried in
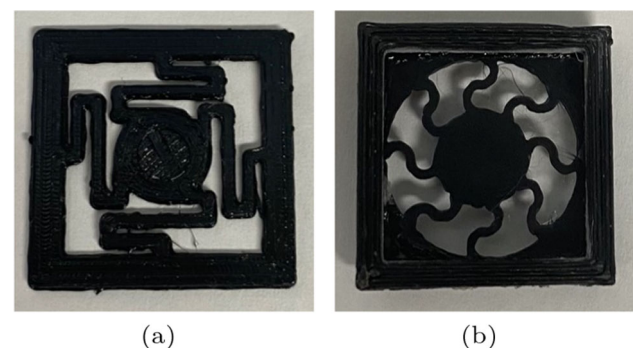

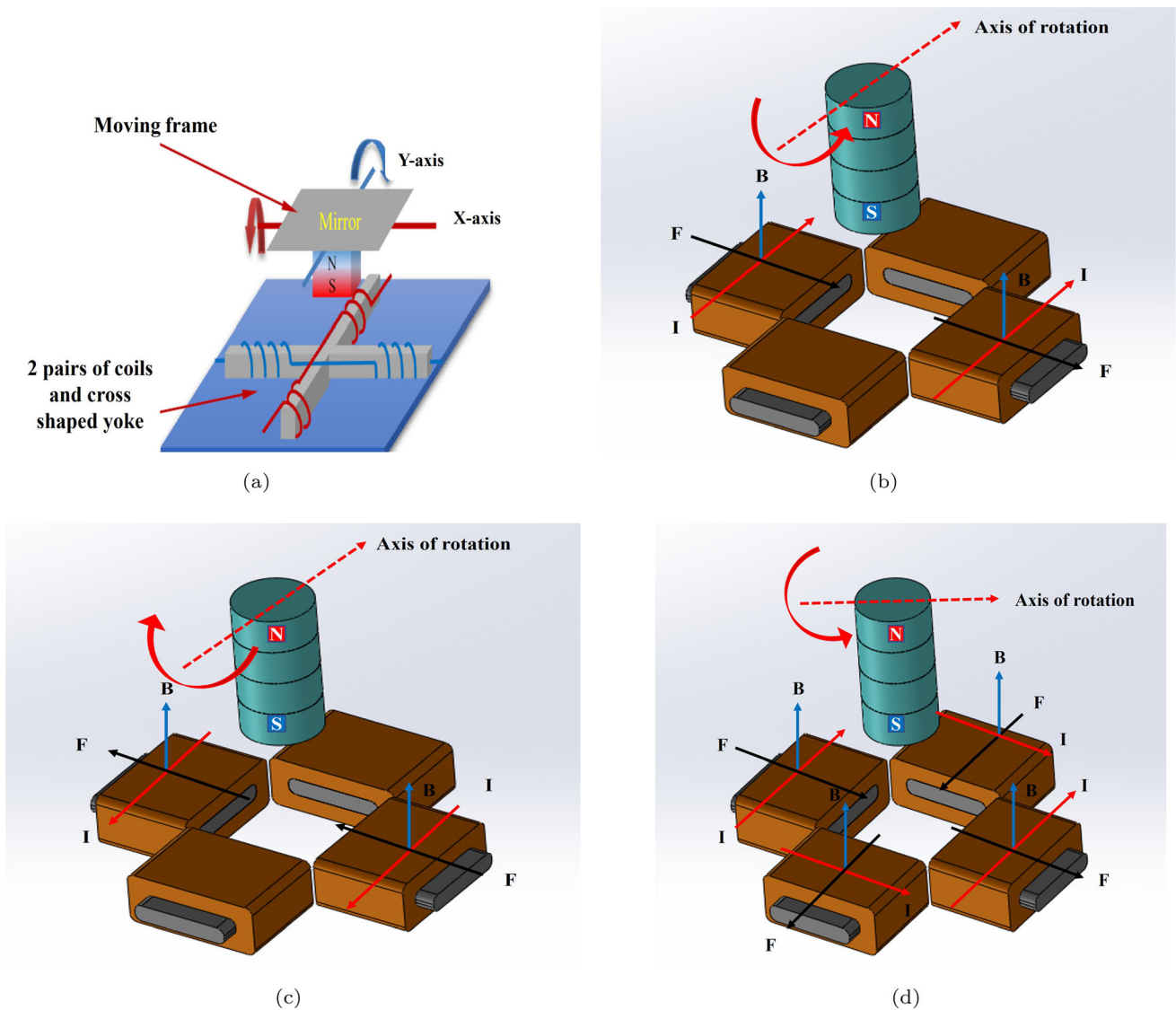**Fig. 2** Proposed flexible membranes: **a** pulse shape, **b** sine shape

Fig. 3 Working principal of the proposed system: Lorentz force (F), magnetic flux (B) and current (I)

Sect. 3. The simulation results are provide the proposed system in Sect. 4. The experimental results and experimental setup are described in Sect. 5. The conclusion is provided in Sect. 6.

2 Design of a scanning micro-mirror

In this study, a 2-DOF scanning mirror was created using flexible membrane and an electromagnetic actuator. Figure 1 represents the 3D model of the proposed system. The overall dimensions of that system are 24 mm (width) × 24 mm (depth) × 20 mm (height). Additionally, here is a moving component at the top of the system and a fixed component at the bottom. The fixed part is composed of a bottom plate, four rigid supports, and two

sets of coils surrounding a single cross-shaped yoke. The moving part consists of a permanent magnet and a flexible membrane with simple and compact structure. In the middle of the flexible membrane, there is a movable plate that serves as a platform to hold a mirror on top. This plate also provides a location for attaching a permanent magnet underneath. To ensure flexibility and movement, elastic beams are used to connect this plate to the exterior structure. These elastic beams enable the plate to move and respond to external forces or actuation, allowing for the desired scanning motion of the mirror.

The flexible compliant membranes are fabricated by 3D printing multiple individual beams using an elastic material. The unique shape of each beam enables the compliant membrane to exhibit excellent compliance in both transnational and rotational degrees of freedom. Figure 2
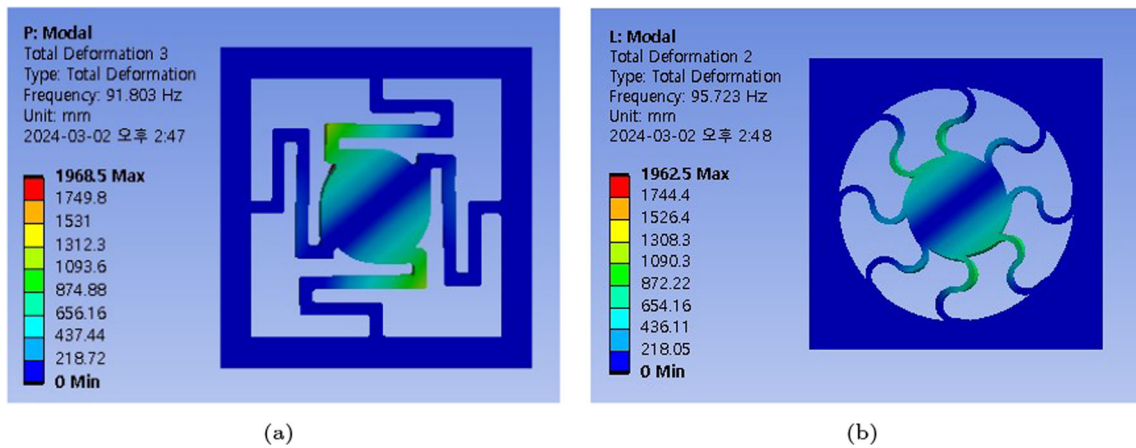
Fig. 4 Simulation results: vibration displacement analysis of the proposed flexible compliant membranes. **a** Pulse shape, **b** sine shape

Table 1 Resonant peak frequencies of displacement in vibration simulation

Flexible compliant membranes	Frequency (Hz)
Pulse shape	92
Sine shape	96

shows the flexible compliant membranes which used in this study. The flexible membranes were fabricated using an elastic filament called "eFlex(TPU)" from the company eSun™. This filament is characterized by a relatively low density of 1.12 g/cm³, contributing to the lightweight nature of the constructed membranes. The filament's Young's modulus is 66 MPa, and its Poisson's ratio is 0.36 (Adrover-Monserrat et al. 2022). Additionally, it demonstrates a high tensile strength of 52 MPa, signifying its capacity to withstand substantial forces without fracturing.

Furthermore, the material exhibits an elongation at break value of 500%, indicating its remarkable flexibility and ability to stretch significantly before reaching its breaking point. These membranes are securely fixed to a plastic square frame. The frame is tightly attached to the stationary frame using four holders on each edge. This design ensures both simplicity and compactness while providing robustness to securely hold the flexible membranes in place.

3 Dynamic model and working principle of the system

The dynamic model of the proposed system is theoretically based on a DC motor. Hence, the dynamic system's equations can be expressed as follows:

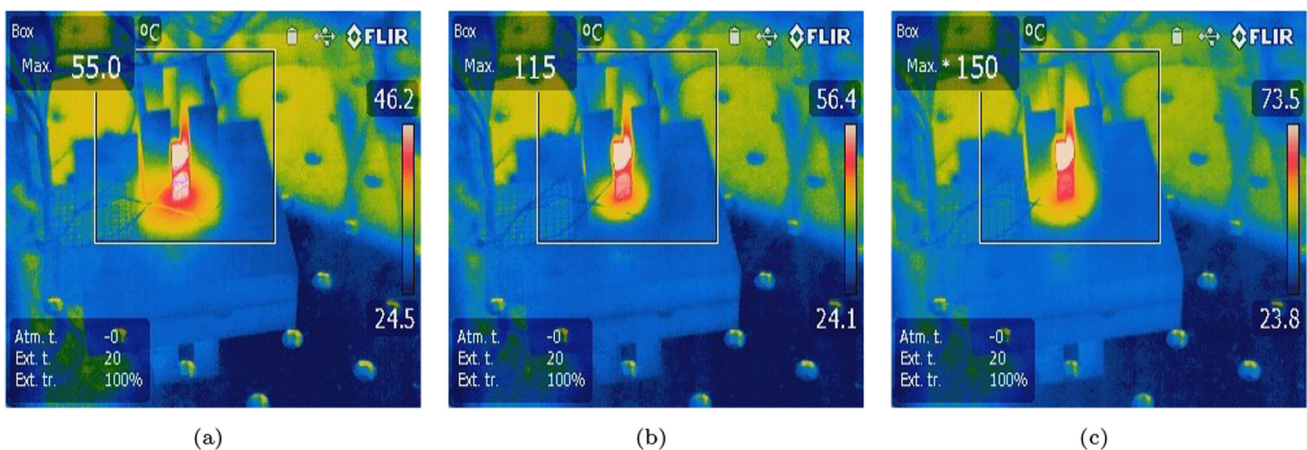$$J\ddot{\theta} + \tau_m = \tau_e \tag{1}$$

Fig. 5 Thermal experiment results: **a** input voltage 5 V, **b** input voltage 8.5 V, **c** input voltage 15 V
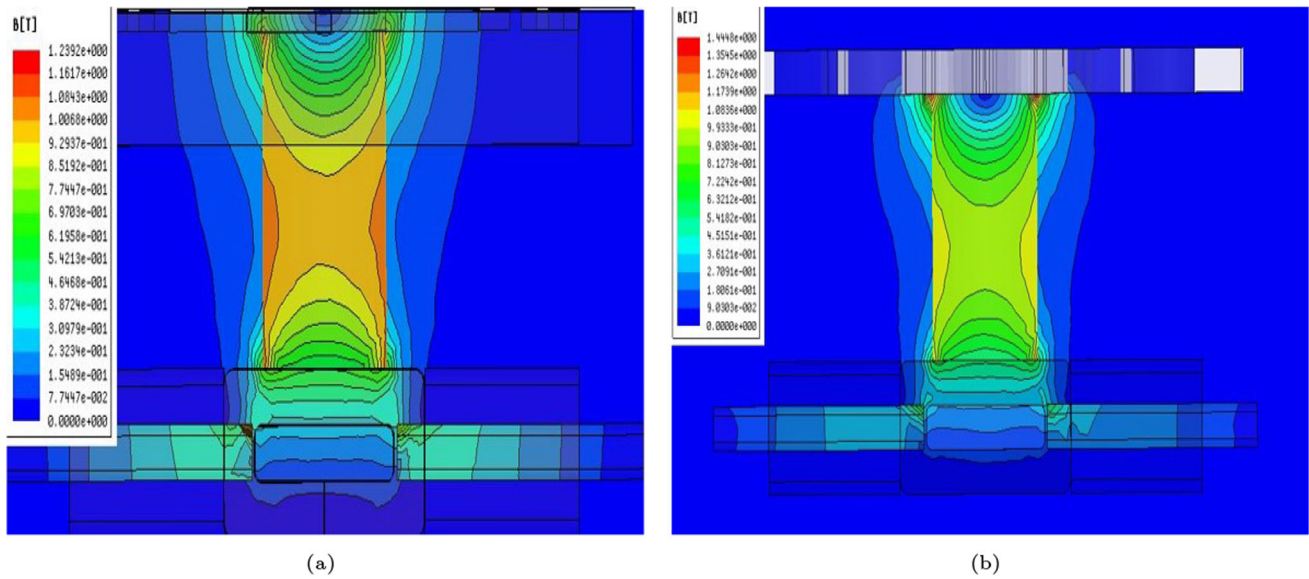
Fig. 6 Simulation results of the magnetic flux density: **a** pulse-shaped, **b** sine-shaped

$$\tau_e = K_t I \tag{2}$$

$$\tau_m = K_m \theta \tag{3}$$

$$V = K_e \dot{\theta} + IR \tag{4}$$

where $J, \ddot{\theta}, \dot{\theta}, \theta$ are the mass moment of inertia, angular acceleration, angular velocity, and rotation angle, respectively. τ_m, τ_e are the restoring torque that brings the permanent magnet back to its neutral position, and the torque that induces the rotation of the permanent magnet to a particular angle, respectively. K_m, K_t, K_e are the restoring, torque, and back-emf constants, respectively. As an assumption, we consider that the force constant and the back-emf constant in the electromagnetic system are usually equivalent to those found in a DC motor. In this context, we represent the input voltage, current, and resistance of the coil as V, I, and R, respectively. However, for simplicity, we neglect the inclusion of the electrical circuit's indicating component in the model. The relationship between the input and output is as follows.

$$\frac{\theta}{V} = \frac{K_t/R}{JS^2 + (K_t K_e/R)S + K_m} \tag{5}$$

In this context, we define the variable V as the input, representing the applied voltage to the system. On the other hand, the variable θ represents the output, specifically the rotation angle of the system.

The mounting point for the permanent magnet was located at the bottom of the central membrane, enabling vertical movement in response to current direction. To achieve rotation along the Y-axis, the upper and lower coils are connected in series and energized with current,

resulting in the mirror rotation as shown in Fig. 3a for the red coils. On the other hand, the left and right coils control the horizontal displacement of the permanent magnet in alignment with the current direction. Furthermore, as represented in Fig. 3a for the blue coils, the mirror undergoes rotation around the X-axis. When using two coils, it becomes possible to rotate either the X-axis or the Y-axis as the rotation axis. As illustrated in the Fig. 3b and c, when current is applied to these two coils, it can be observed that the Y-axis rotates and serves as the rotation axis. The direction of the Lorentz force is determined by the direction of the current, thereby providing the ability to select the desired rotation direction. By using the four coils, it is possible to achieve diagonal movement. As represented by Fig. 3d, when an equal amount of current is applied to each of the four coils, a resultant force is generated in the 45° direction, which lies between the Y-axis and the X-axis. This force enables rotation around the axis indicated by the dotted line. By adjusting the magnitude of the current, it is feasible to set the axis at different angles as desired.

4 Simulation results

The frequency response of an electromechanical system is a critical factor in assessing its performance. In order to evaluate the proposed system, a finite analysis simulation was conducted. The simulation results of the vibration displacement for the compliant membranes are depicted in Fig. 4. Additionally, Table 1 presents the frequencies at which displacement resonant peaks occur. Among the both shapes that were considered, the design featuring sine
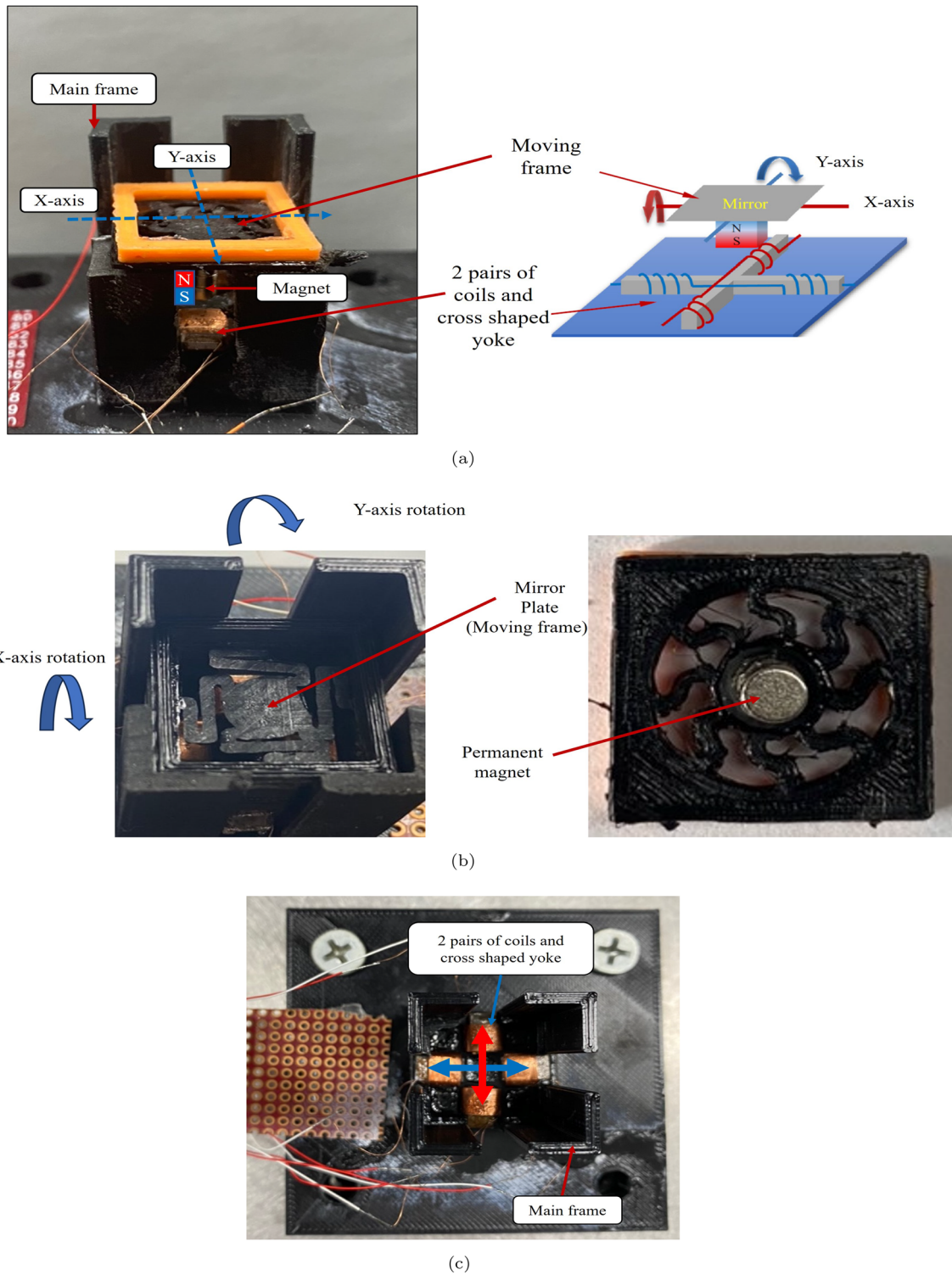
(a)

(b)

(c)

Fig. 7 System structure: **a** manufactured system, **b** moving frame, **c** main frame

shape exhibits the highest frequency response. This particular design achieves a maximum frequency of 96 Hz, surpassing the other proposed shape in terms of its ability to respond to higher frequencies.

During the actuator manufacturing process, it was crucial to ensure that the heat generated did not reach temperatures that could cause the bond or PLA (polylactic acid) material to melt. To assess the heat generated, voltages of 5 V, 8.5 V, and 15 V were applied as shown in
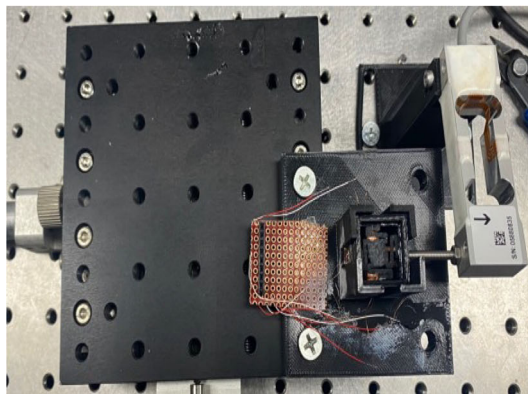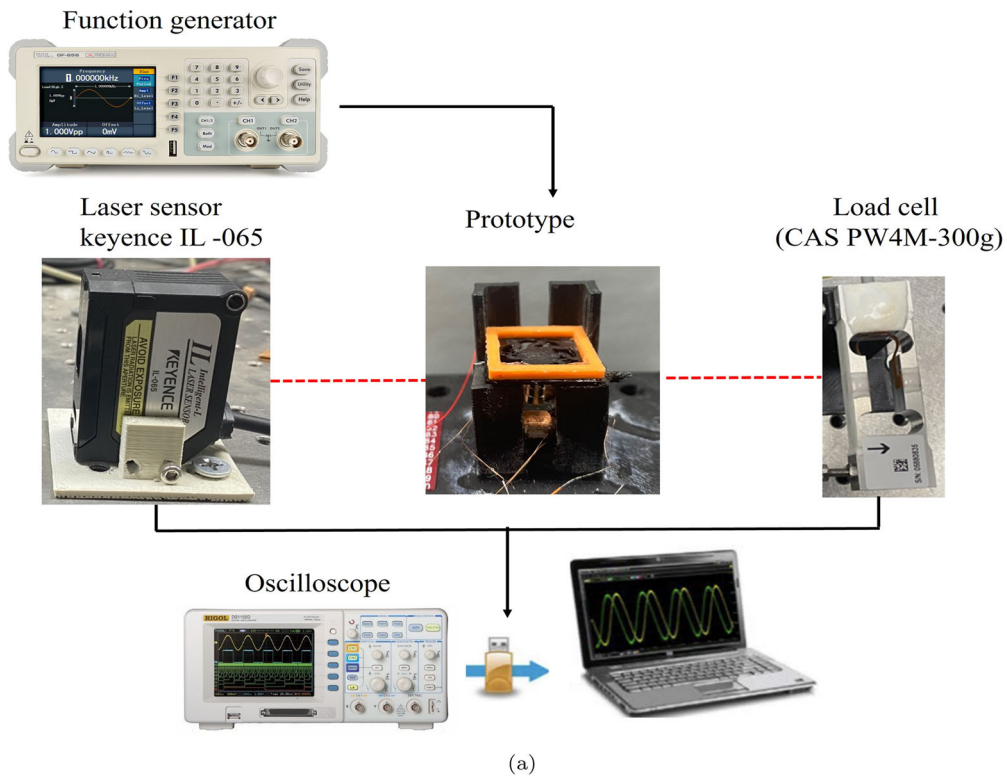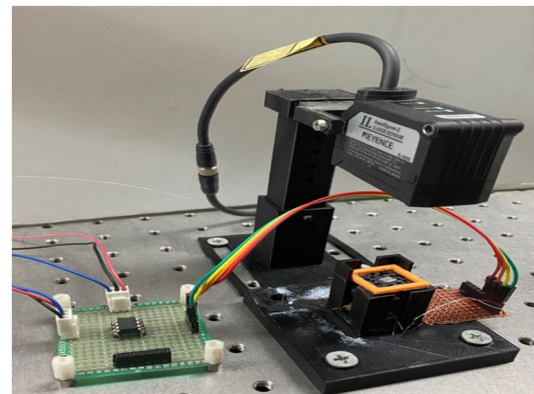
Fig. 8 a Experimental setup, **b** torque measurement, **c** motion angel measurement

Fig. 5. Considering the melting temperature of the bond at 135 °C and the melting temperature of PLA at 180 °C, a voltage of 5 V was selected to ensure that the heat generated remained below 55 °C. This choice was made to maintain a safe and constant operating temperature for the actuator.

Figure 6 presents the magnetic flux density simulation results, with input current of 10 mA. This visualization provides valuable insights into the behavior of the system under these specific conditions.
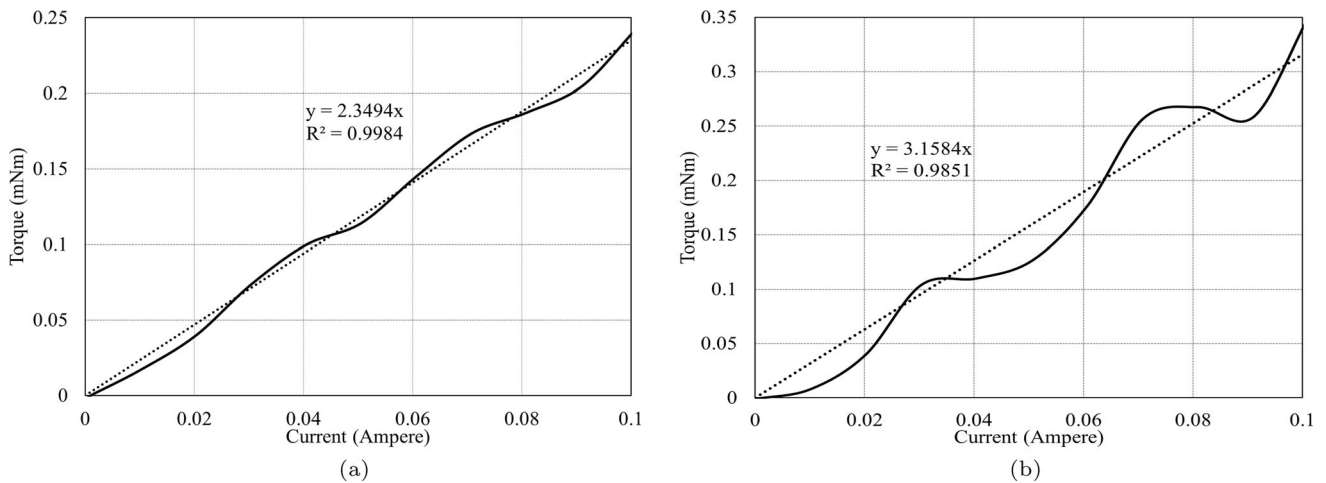
Fig. 9 Simulation results: torque constant, **a** pulse-shaped, **b** sine-shaped
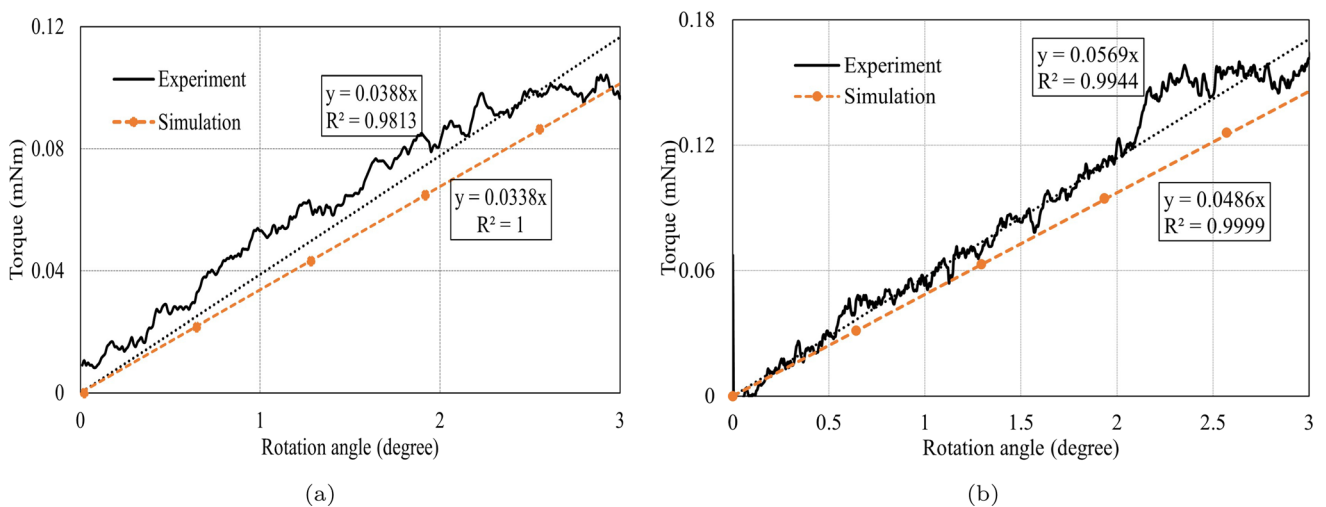

Fig. 10 Simulation and experimental results: restoring constant, **a** pulse-shaped, **b** sine-shaped
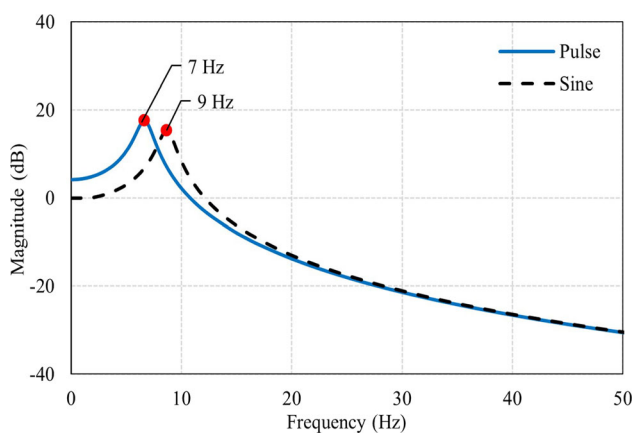

Fig. 11 Simulation results: dynamic response

5 Experiment of the scanning micro-mirror

5.1 Experimental setup

Figure 7 represent the manufactured prototype. That mirror has a circle shape with a radius of 3 mm which is attached to the flexible membrane. While the overall dimensions of that system are 24 mm (width) × 24 mm (depth) × 20 mm (height). The permanent magnet material was Neodymium (ND45). The base coil comprises 810 turns and a resistance of 58 Ω. The yoke with the cross shape of the base coil was made of steel (S45C). The experimental setup was shown in Fig. 8. We controlled the system by implementing an open loop control circuit that utilized a power op-amp. We used to generate the input signal by function generator. As shown in Fig. 8b, the torque of the mirror and the frame are measured by using a load cell (CAS PW4M-300g). Figure 8c shows a laser
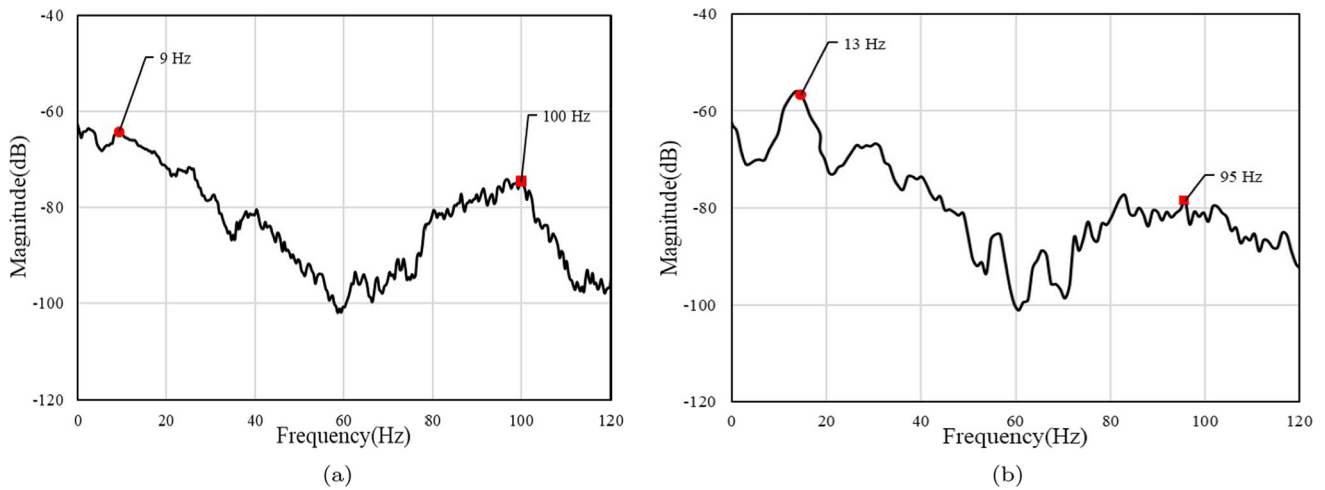
Fig. 12 Experimental results: dynamic response, **a** pulse-shaped, **b** sine-shaped
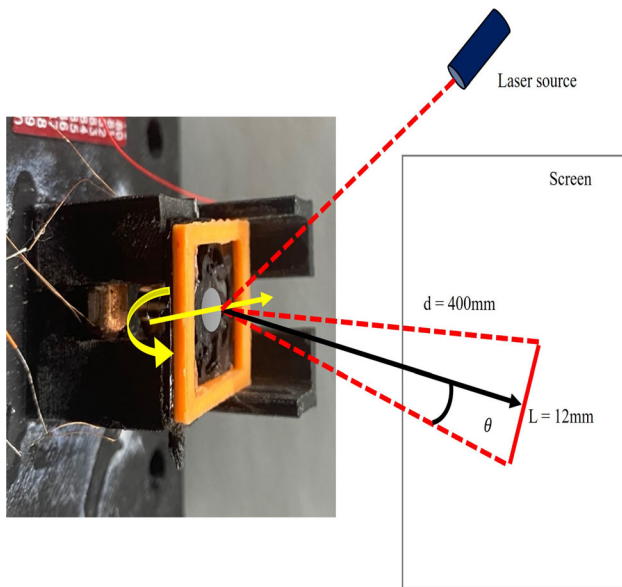

Fig. 13 Schematic diagram illustrating the optical scan angle measurement method

displacement sensor (Keyence IL-065) that is used to measure the mirror displacement. We have measured the vertical motion of the mirror at the corners of it, which are 3 mm away from its center. We calculated the rotation angle using trigonometric functions.

5.2 Experimental results

The simulated torque of the proposed system with both membrane was represented in Fig. 9. Figure 9a representing the simulated torque of the proposed system with a sine-shaped membrane, while Fig. 9b representing the simulated torque of the system with a pulse-shaped mem-

brane. The torque constant K_t is calculated using Eq. 2 and it is determined by calculating the slope of the lines in the plotted data. From the simulated data with a sine-shaped membrane, the value of K_t is found to be 2.349 mNm/A, while with a pulse-shaped membrane the value of K_t is 3.158 mNm/A.

The experimental and FEA simulation results of the proposed system with a sine-shaped membrane and a pulse-shaped membrane are shown in Fig. 10a and b respectively, which shows the simulated and measurement of restoring constant of the proposed system with a sine-shaped membrane and a pulse-shaped. The restoring constant K_m is calculated using Eq. 2, which is proportional to the angle. The constant is determined by calculating the slope of the lines in the plotted data. In Fig. 10a and b the experimental results were represented by solid lines while the simulation results were represented by dashed lines. From the simulated and experimental data with a pulse-shaped membrane, the value of K_m is found to be 0.0388 mNm/degree for both data. Similarly From the simulated and experimental data with a sine-shaped membrane, the value of K_m is found to be 0.0486 mNm/degree and 0.0569 mNm/degree, respectively. Despite the nonlinearity and sensitivity of the design parameters, the coefficients of determination R^2 were nearly equal to one. Both the experimental results and simulation results demonstrate that the proposed system can be considered a valid linearized dynamic model.

Figure 11 depicts the theoretical frequency responses of the proposed system, obtained using Eq. 5. The dynamic resonance frequency of the system is 7 Hz when a pulse-shaped membrane is used, and it is 9 Hz when a sine-shaped membrane is employed. These values correspond to the peak values observed in Fig. 11. Measurements were
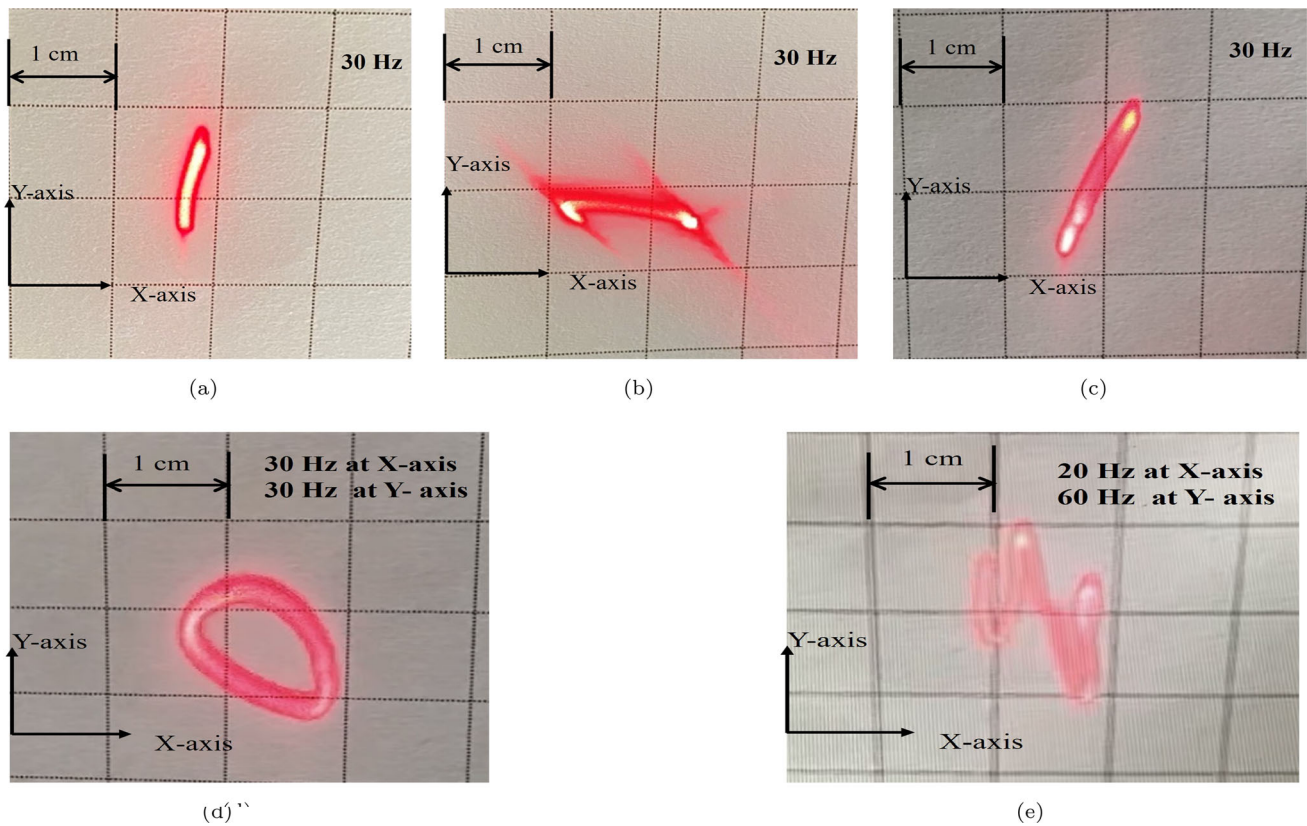
Fig. 14 Laser scanning configurations: **a** vertical, **b** horizontal, **c** diagonal, **d** circle, **e** Lissajous curve

carried out of the developed system's dynamic responses in order evaluate its rotation angle at resonance frequency. Experiments with sinusoidal sweep excitation were performed experimentally to determine the dynamic response. The frequency range of the sine sweep signal was 1–100 Hz, while the input voltage remained constant at 5 V. Fig. 12 shows the experimental results of the proposed system with both of membranes. The system using a pulse-shaped membrane achieves a rotation angle $\pm 3°$ at resonance frequency of 9 Hz with, the bandwidth of 15 Hz. Additionally at mechanical resonance frequency of 100 Hz the system achieves an angle $\pm 1°$ as shown in Fig. 12a. Figure 12b representing the experimental results of the proposed system using a sine-shaped membrane. At a resonance frequency of 13 Hz, the maximum rotation angle achieved $\pm 2.5°$, with a bandwidth of 19 Hz. Moreover, at a mechanical resonance frequency of 95 Hz, the system achieves $\pm 1°$. The experimental frequencies were observed to be slightly higher than the theoretical values. However, considering the presence of noise in the dynamic response, this difference was acceptable.

The laser beam aimed at the mirror to measure the reflection angle of the developed device as shown in Fig. 13. Furthermore, the trigonometric functions are used to calculate the rotation angle, which is double of the

mirror's optical reflection angle. The mirror's reflection of the laser beam creates several scanning profiles on a graph paper-covered screen. Figure 14 shows that the proposed scanning mirror to adopt different driving patterns at input voltages of ± 5 V at X-axis and ± 5 V at Y-axis. Vertical and horizontal beam patterns were scanned to validate the performance of the proposed scanning mirror. Figure 14a and b show the scanning vertical and horizontal beam profiles, respectively. Figure 14 c show an oscillating line that followed a diagonal oblique trajectory. Figure 14d and e represented the circle and Lissajous curves.

6 Conclusion

This work entails the use of electromagnetic actuator comprised of one magnet and two pairs of coils and cross shaped yoke to develop a 2-D scanning mirror system. The proposed electromagnetic actuator is combined using a mirror-actuating device which can govern the 2-D scanning motion, to rotate the mirror. We have developed two flexible membranes with a simple and compact structure using 3D printing technology. One membrane is designed with a sine shape, while the other features a pulse shape. Furthermore, we conducted experiments with the proposed

system with dimensions of 24 mm (width) × 24 mm (depth) × 20 mm (height), which corresponds to a mirror with a radius of 3 mm. The FEA simulation as well as experimental results validate the effectiveness of the developed system in achieving a broad dynamic range, moderate bandwidth, and large reflection angle at both orthogonal directions to guarantee a better static performance. The maximum rotation angle achieved is ± 3°, with a bandwidth of 15 Hz. Moreover, at a mechanical resonance frequency of 100 Hz, the system achieves an angle of ± 1°. However the rotation angle achieved by our system is relatively small compared to the exciting system, it is important to note that our system was developed with a simple and compact structure using 3D printing technology. In future work, we aim to enhance the system to increase the rotation angle.

Author contributions Conceptualization, methodology, validation, formal analysis, visualization, writing original draft, writing review, editing, submission Sh.M.; methodology, formal analysis, visualization, software, data curation, Y. I.; writing, and editing E. A; review, provided advice, Y.K. and W. K.; supervision, review, editing, resources, funding, principal investigator, project administration B.S.

Data availibility No datasets were generated or analysed during the current study.

Declarations

Conflict of interest All authors certify that they have no affiliations with or involvement in any organization or entity with any financial interest or non-financial interest in the subject matter or materials discussed in this manuscript. The authors declare no Conflict of interest.

References

Adrover-Monserrat B, Llumà J, Jerez-Mesa R, Travieso-Rodriguez JA (2022) Study of the influence of the manufacturing parameters on tensile properties of thermoplastic elastomers. Polymers 14(3):1–13. https://doi.org/10.3390/polym14030576

Anderson NK, Fleming BT, Suresh A, Vorobiev D, Diaz A, France K, Schindhelm R, Hendrix A (2021) Testing and verification of micro-electro-mechanical systems (MEMS) micromirrors for high-performance scientific applications. UV, X-ray, and gamma-ray space instrumentation for astronomy XXII, Vol 11821. SPIE, pp 331–345

Chen S, Zhang Y, Hong X, Li J (2022) Technologies and applications of silicon-based micro-optical electromechanical systems: a brief review. J Semicond 43(8):081301

Cheng H-C, Liu S-C, Hsu C-C, Lin H-Y, Shih F, Wu M, Liang K-C, Lai M-F, Fang W (2023) On the design of piezoelectric MEMS scanning mirror for large reflection area and wide scan angle. Sens Actuators A Phys 349:114010

Conant RA, Hagelin PM, Krishnamoorthy U, Hart M, Solgaard O, Lau KY, Muller RS (2000) A raster-scanning full-motion video display using polysilicon micromachined mirrors. Sens Actuators A Phys 83(1–3):291–296

Csencsics E, Schitter G (2017) System design and control of a resonant fast steering mirror for Lissajous-based scanning. IEEE/ASME Trans Mechatron 22(5):1963–1972

Fan Y, Ma W, Jiang P, Huang J, Chen K, Pan N (2019) Improving angular accuracy of a scanning mirror based on error modeling and correction. Sensors 19(2):367

Gilchrist KH, McNabb RP, Izatt JA, Grego S (2009) Piezoelectric scanning mirrors for endoscopic optical coherence tomography. J Micromech Microeng 19(9):095012

Gilchrist KH, Dausch DE, Grego S (2012) Electromechanical performance of piezoelectric scanning mirrors for medical endoscopy. Sens Actuators A Phys 178:193–201

Huang C-H, Yao J, Wang LV, Zou J (2013) A water-immersible 2-axis scanning mirror microsystem for ultrasound andha photoacoustic microscopic imaging applications. Microsyst Technol 19:577–582

Hung AC-L, Lai HY-H, Lin T-W, Fu S-G, Lu MS-C (2015) An electrostatically driven 2D micro-scanning mirror with capacitive sensing for projection display. Sens Actuators A Phys 222:122–129

Hwang J-Y, Yarar E, Wysocki L, Röhr F, Wille G, Gu-Stoppel S (2024) Low-power multi-scan patterns capable 3D-constructed piezoelectric MEMS mirrors. In: MOEMS and miniaturized systems XXIII, Vol 12899. SPIE, pp 88–95

Hyun SB, Dongho O, Lee S-Y (2013) A two-dimensional laser scanning mirror using motion-decoupling electromagnetic actuators. Sensors 13(4):4146–4156

Ito S, Csencsics E, Schitter G (2023) Modeling-free learning control of cross-coupled fast steering mirror for 2-D trajectory. IFAC-PapersOnLine 56(2):5340–5345

Jin J-Y, Park J-H, Yoo B-W, Jang Y-H, Kim Y-K (2011) Numerical analysis and demonstration of a 2-DOF large-size micromirror with sloped electrodes. J Micromech Microeng 21(9):095006

Khatokar JA, Vinay N, Bale AS, Nayana MA, Harini R, Reddy VS, Soundarya N, Satheesha TY, Huddar AS (2021) A study on improved methods in Micro-electromechanical systems technology. Mater Today Proc 43:3784–3790

Koh KH, Lee C (2012) A two-dimensional MEMS scanning mirror using hybrid actuation mechanisms with low operation voltage. J Microelectromech Syst 21(5):1124–1135

Koh KH, Kobayashi T, Lee C (2011) A 2-D MEMS scanning mirror based on dynamic mixed mode excitation of a piezoelectric PZT thin film S-shaped actuator. Opt Express 19(15):13812–13824

Mao H, Dong X, Liu Y (2022) A subwavelength-grating-mirror-based MEMS tunable Fabry–Perot filter for hyperspectral infrared imaging. J Microelectromech Syst 32(1):57–66

Mao H, Dong X, Liu Y, Silva KKMBD, Faraone L (2022) A suspended metamaterial mirror for hyperspectral shortwave infrared Fabry–Perot filters. J Microelectromech Syst 31(4):644–652

Mohamed S, Im Y, Shin H, Kim Y, Shin B (2024) Design, modeling, and simulation of a novel electromagnetic linear actuator for linear motion. IEEE Access 12:38899–38907. https://doi.org/10.1109/ACCESS.2024.3375887

Qi W, Chen Q, Guo H, Xie H, Xi L (2018) Miniaturized optical resolution photoacoustic microscope based on a microelectromechanical systems scanning mirror. Micromachines 9(6):288

Sadhukhan D, Singh GP (2022) Design of electrostatic actuated MEMS biaxial scanning micro-mirror with serpentine structure. Mater Today Proc 65:229–234

Samanta BR, Pardo F, Salamon T, Kopf R, Eggleston MS (2022) Low-cost electrothermally actuated MEMS mirrors for high-speed linear raster scanning. Optica 9(2):251–257

Senger Frank, Gu-Stoppel Shanshan, Wen Lianzhi, Albers Jörg, Timmermann Marec, Bruns Stefan, Piechotta Gundula, Buenting Udo, Schulz-Ruhtenberg Malte (2021) A 2D circular-scanning piezoelectric MEMS mirror for laser material processing. In: MOEMS and miniaturized systems XX, Vol 11697. SPIE, pp 14–22

Shin B, Oh D, Lee K (2018) Biaxial scanning mirror with large rotation angle and low resonance frequency for LIDAR application. Microsyst Technol 24:4631–4639

Tanguy QAA, Bargiel S, Xie H, Passilly N, Barthès M, Gaiffe O, Rutkowski J, Lutz P, Gorecki C (2017) Design and fabrication of a 2-axis electrothermal mems micro-scanner for optical coherence tomography. Micromachines 8(5):146

Yalcinkaya AD, Urey H, Brown D, Montague T, Sprague R (2006) Two-axis electromagnetic microscanner for high resolution displays. J Microelectromech Syst 15(4):786–794

Yangyang W, Qian K-Y (2019) 2-D scanning LiDAR with MEMS mirror and STM32. IOP Conf Ser Mater Sci Eng 563(3):032051

Yu H, Zhou P, Shen W (2021) Fast-scan MOEMS mirror for HD laser projection applications. In: 2021 IEEE 16th international conference on nano/micro engineered and molecular systems (NEMS). IEEE, pp 265–269

Zara JM, Yazdanfar S, Rao KD, Izatt JA, Smith SW (2003) Electrostatic micromachine scanning mirror for optical coherence tomography. Opt Lett 28(8):628–630

Zhang WR, Cheng L, Wu SY, Ji YC, Li C, Fang GY (2023) Mid-range 2-D fast imaging in pseudo-polar coordinate format for wideband array. IEEE Antennas Wirel Propag Lett 22(10):2590–2594

Zhou G, Lim ZH, Qi Y, Chau FS, Zhou G (2021) MEMS gratings and their applications. Int J Optomechatron 15(1):61–86